

## Research Article

## Open Access

Alessandro De Rosi\*

# Non-linear flow-induced vibrations in deformable curved bodies: A lattice Boltzmann-immersed boundary-finite element study

DOI 10.1515/cls-2015-0018

Received April 10, 2015; accepted May 15, 2015

**Abstract:** The dynamic response of a deformable curved solid body is investigated as it interacts with a flow field. The fluid is assumed to be viscous and the flow is nearly incompressible. Fluid dynamics is predicted through a lattice Boltzmann solver. Corotational beam finite elements undergoing large displacements are adopted to idealize the submerged body, whose presence in the lattice fluid background is handled by the immersed boundary method. The attention focuses on the solid's deformation and a numerical campaign is carried out. Findings are reported in terms of deformation energy and deformed configuration. On the one hand, it is shown that the solution of the problem is strictly dependent on the elastic properties of the body. On the other hand, the encompassing flow physics plays a crucial role on the resultant solid dynamics. With respect to the existing literature, the present problem is attacked by a new point of view. Specifically, the author proposes that the problem is governed by four dimensionless parameters: the Reynolds number, the normalized elastic modulus, the density and aspect ratio. The formulation and the solution strategy for curved solid bodies herein adopted are introduced for the first time in this paper.

**Keywords:** Fluid-structure interaction, Curved bodies, Lattice Boltzmann method, Immersed Boundary method

## 1 Introduction

Slender thin walled structures are widely used in naval and ocean engineering [1–4]. Due to the interaction with the surrounding fluid environment, these structures can

undergo non-linear forced vibrations, which should be accounted for and properly computed in order to address a safe and stable design of the mechanical components. Natural and forced vibrations of curved bodies have been widely investigated by several authors, by considering functionally graded [5, 6], composite laminated [7–10], orthotropic [11] and even isotropic materials [12–14]. Moreover, a huge attention has been devoted to the vibrations of cylindrical bodies filled with an inviscid fluid [15, 16]. In [17–20] an in-depth discussion is provided concerning the non-linear dynamics of simply supported cylindrical bodies. The effects of the flow compressibility have been discussed in [21, 22]. In [23, 24] the role of structural imperfections on the structural stability has been highlighted. In [25, 26] the response to shock waves has been investigated. Moreover, natural vibrations of non-circular solids conveying a fluid have been elucidated in [27]. In addition, an interesting topic is represented by the prediction of the behaviour of structures interacting with a flowing fluid [28–30]. In fact, the resultant vibration regime exhibits marked non-linear and non-stationary features [31–33]. For instance, chaotic non-linear oscillations can affect a thin plate interacting with a flow [34, 35]. To the author's best knowledge, limited previous efforts concerning the unsteady response of curved bodies interacting with a viscous fluid have been found. Its accurate prediction represents a compelling challenge, since the time-dependent dynamics of a submerged body strictly depends on the flow characteristics, on the one hand, and on the solid mechanical properties, on the other hand. Therefore, the combination of a solution strategy for unsteady viscous fluid dynamics with one for unsteady solid dynamics represents an added value to existing literature.

In this paper, the author proposes a numerical approach for computing the non-stationary non-linear dynamics of curved bodies immersed in a viscous fluid. A numerical campaign is performed by varying the flow and solid properties. Specifically, it is proposed that the problem is governed by four dimensionless: the Reynolds number  $\mathcal{R}$ , the dimensionless elastic modulus  $\mathcal{E}$ , the density ratio  $\mathcal{D}$

\*Corresponding Author: Alessandro De Rosi: Laboratoire de Mécanique des Fluides et d'Acoustique, Ecole Centrale de Lyon, 36 avenue Guy de Collongue, 69134 Ecully cedex, France, E-mail: alessandro.de-roisi@ec-lyon.fr.

and the aspect ratio  $\mathcal{H}$ , as specified in the next section. The flow physics is predicted through the lattice Boltzmann (LB) method [36–39]. In the last decades, the LB method has attracted a growing attention among scientists involved in the computational fluid dynamics framework. Presently, it represents a accurate, effective, efficient, and robust alternative to classical continuum-based solvers. To account for the presence of an immersed curved solid body, here the Immersed Boundary (IB) method [40–43] is employed. Such method has been preferred to the well consolidated interpolated bounce-back scheme [44] for two reasons. The former is that it possesses superior properties in terms of stability and involved computational effort [45]. The latter is that the solid mesh is totally independent of the fluid one. Therefore, a general algorithm for handling a solid body can be developed. Once the forces that the fluid exerts upon the immersed body are computed, its position is updated in time by solving the equation of the solid motion. In particular, the solid surface is idealized by corotational beam finite elements undergoing large displacements [46, 47] and the resultant nonlinear equation of the solid motion is solved by adopting the time discontinuous Galerkin (TDG) scheme. The numerical algorithm combining the above mentioned methods has proved to represent a robust, effective and accurate tool able to simulate a large set of fluid-structure interaction phenomena [48–51].

The paper is organized as follows. In Section 2, the problem is stated and the adopted numerical methods are briefly recalled. In Section 3, results of a numerical campaign are discussed. Some conclusions are drawn in Section 4. Finally, a validation is provided in Appendix.

## 2 Problem statement

Making reference to Figure 1, a clamped-clamped slender curved solid body (blue line) is immersed in a quiescent viscous fluid of density  $\rho$  and kinematic viscosity  $\nu$ . The

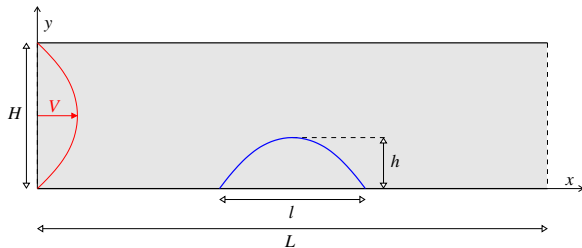


**Figure 1:** Sketch of the problem definition. The channel has length  $L = 300$  and  $H = 60$  (in lattice units).

body possesses mass per unit length  $m$ , mass density  $\rho_s$ , cross-sectional area  $A$  and inertia  $J$ . The horizontal projection of the length is denoted by  $l$ . The central point of the body is aligned with the center of the fluid domain in the horizontal direction. The equations of the solid motion read as follows:

$$EJ \frac{\partial^4 d_y}{\partial x^4} + m \frac{\partial^2 d_y}{\partial t^2} = -q_y(x), \quad (1)$$

$$EA \frac{\partial^4 d_x}{\partial x^4} - m \frac{\partial^2 d_x}{\partial t^2} = -q_x(x). \quad (2)$$

The displacements  $d_x$  and  $d_y$  are parallel and normal to the centroidal axis of the beam,  $x$ , respectively; in such directions, the external loads  $q_x(x)$  and  $q_y(x)$  act upon the structure. As usual, the time is denoted by  $t$ .

The flow physics is predicted by solving the Navier-Stokes equations for an incompressible flow, which can be written as

$$\nabla \cdot \mathbf{u} = 0, \quad (3)$$

$$\frac{\partial \mathbf{u}}{\partial t} + (\mathbf{u} \cdot \nabla) \mathbf{u} = -\frac{1}{\rho} \nabla p + \nu \nabla^2 \mathbf{u}, \quad (4)$$

where  $\mathbf{u}$  is the flow velocity and  $p$  is the fluid pressure. At  $y = 0$  and  $y = H$ , the no-slip condition  $\mathbf{u} = 0$  is enforced. At  $x = 0$  a parabolic constant uniform rightward velocity profile of peak value  $V$  is assigned, whereas at  $x = L$  outflow conditions are prescribed. The no-slip condition at the fluid-solid interface completes the definition of the problem.

The author proposes that it is governed by the following dimensionless parameters: the Reynolds number  $\mathcal{R} = \frac{VL}{\nu}$ , the dimensionless elastic modulus  $\mathcal{E} = \frac{E}{\rho V^2}$ , the density ratio  $\mathcal{D} = \frac{\rho_s}{\rho}$  and the aspect ratio  $\mathcal{H} = \frac{h}{l}$ ,  $h$  being the  $y$  coordinate of the solid topmost point.

### 2.1 Numerical methods

By adopting the two-dimensional D2Q9 model [38], the lattice BGK equation is solved on a fixed square grid, thus computing the space-time evolution of the particle distribution functions  $f_i$ , which are forced to move along nine prescribed directions  $i$  with velocities  $\mathbf{c}_i$ . This equation reads as follows:

$$f_i(\mathbf{x} + \Delta t \mathbf{c}_i, t + \Delta t) = f_i(\mathbf{x}, t) + \frac{1}{\tau} [f_i^{eq}(\mathbf{x}, t) - f_i(\mathbf{x}, t)] + \Delta t F_i, \quad (5)$$

where  $\mathbf{x}$  is the position,  $\Delta t$  is the time step and  $\tau$  is the so-called relaxation parameter. It is worth to notice that the relaxation parameter  $\tau$  is strictly related to the fluid viscosity as  $\nu = (\tau - 1/2) c_s^2$ , being  $c_s^2 = \sum w_i \mathbf{c}_i^2 = 1/3$  with  $w_i$  a set of 9 weights defined as  $w_0 = 4/9$ ,  $w_1 = w_2 = w_3 =$

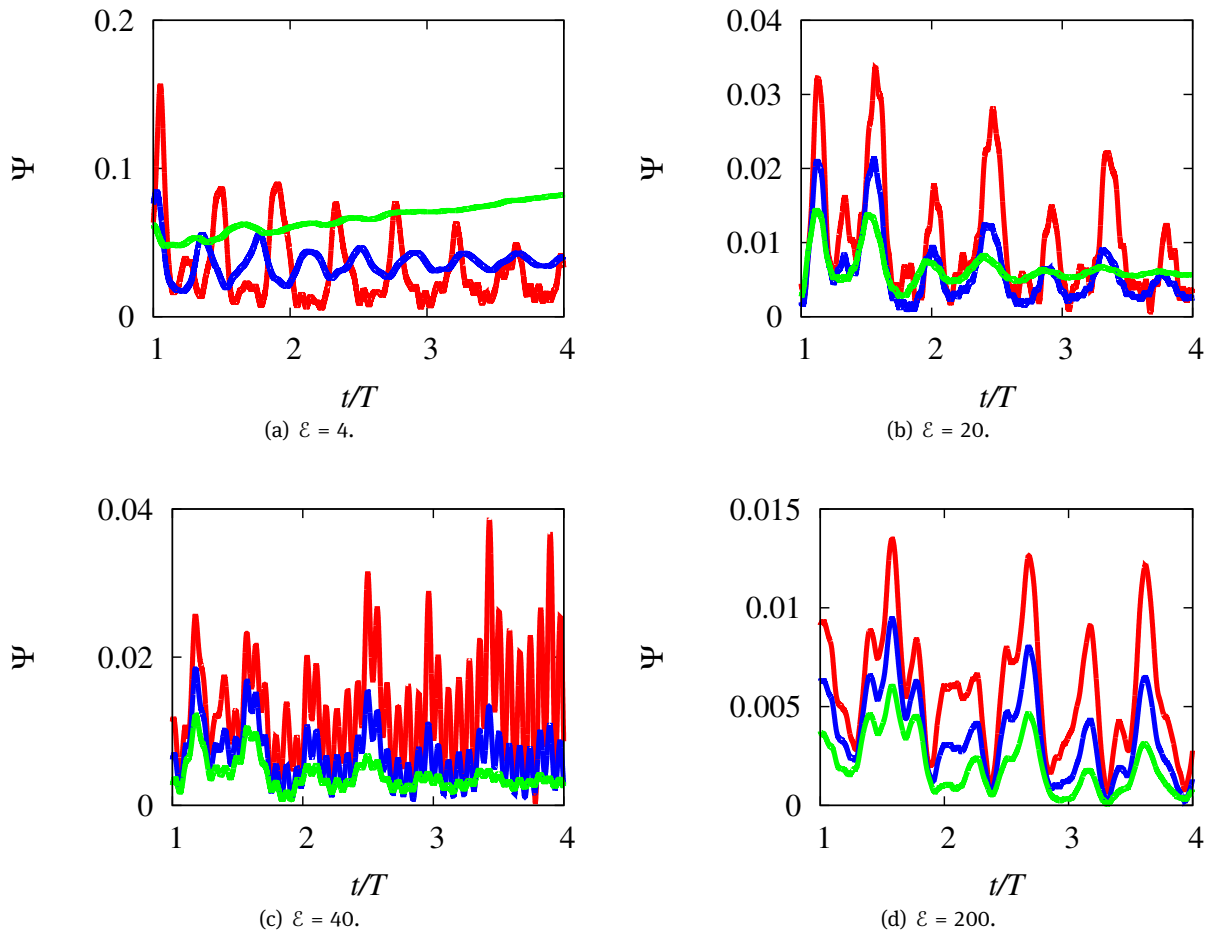


**Figure 2:** Time history of the deformation energies for different values of  $\varepsilon$  at  $\mathcal{R} = 15$  (green curve),  $\mathcal{R} = 50$  (blue curve) and  $\mathcal{R} = 100$  (red curve).

$w_4 = 1/9$  and  $w_5 = w_6 = w_7 = w_8 = 1/36$ . By performing a second-order expansion in the local Mach number [37], the equilibrium particle distribution functions  $f_i^{eq}$  can be computed as

$$f_i^{eq} = w_i \rho \left[ 1 + \frac{\mathbf{v} \cdot \mathbf{c}_i}{c_s^2} + \frac{(\mathbf{v} \cdot \mathbf{c}_i)^2}{2c_s^4} - \frac{\mathbf{v} \cdot \mathbf{v}}{2c_s^2} \right]. \quad (6)$$

The macroscopic fluid density  $\rho$  and the flow velocities  $\mathbf{v}$  can be computed as

$$\rho = \sum_i f_i, \quad \rho \mathbf{v} = \sum_i f_i \mathbf{c}_i, \quad (7)$$

respectively. In order to account for the presence of the body in the fluid lattice background, the Immersed Boundary method [41] is adopted. The term  $F_i$  is a discrete force distribution allowing to account for the body force boundary-induced  $\mathbf{g}$  as follows

$$F_i = \left( 1 - \frac{1}{2\tau} \right) w_i \left[ \frac{\mathbf{c}_i - \mathbf{v}}{c_s^2} + \frac{\mathbf{c}_i \cdot \mathbf{v}}{c_s^4} \mathbf{c}_i \right] \cdot \mathbf{g} \quad (8)$$

The IB is adopted in an implicit velocity-correction strategy, leading to a correction term  $\mathbf{g}$ . Then, the corrected flow velocity  $\mathbf{v}^*$  is determined as follows

$$\rho \mathbf{v}^* = \sum_i f_i \mathbf{c}_i + \frac{1}{2} \Delta t \mathbf{g}. \quad (9)$$

Once fluid forces are computed, the finite element solver is adopted to update the solid position. Slender and geometrically non-linear two-nodes beam finite elements are employed to discretise the structure. Large displacements are accounted for through the corotational formulation. The resultant non-linear equation of solid motion reads as follows

$$\mathbf{M} \ddot{\mathbf{U}} + \mathbf{S}(\mathbf{U}) = \mathbf{F}(\mathbf{U}), \quad (10)$$

being  $\mathbf{M}$  the mass matrix,  $\mathbf{S}(\mathbf{U})$  and  $\mathbf{F}(\mathbf{U})$  the internal and external force vectors, respectively, depending on the vector of nodal displacements  $\mathbf{U}$ . Superimposed dots indicate the time derivative. Equation (10) is integrated in time by

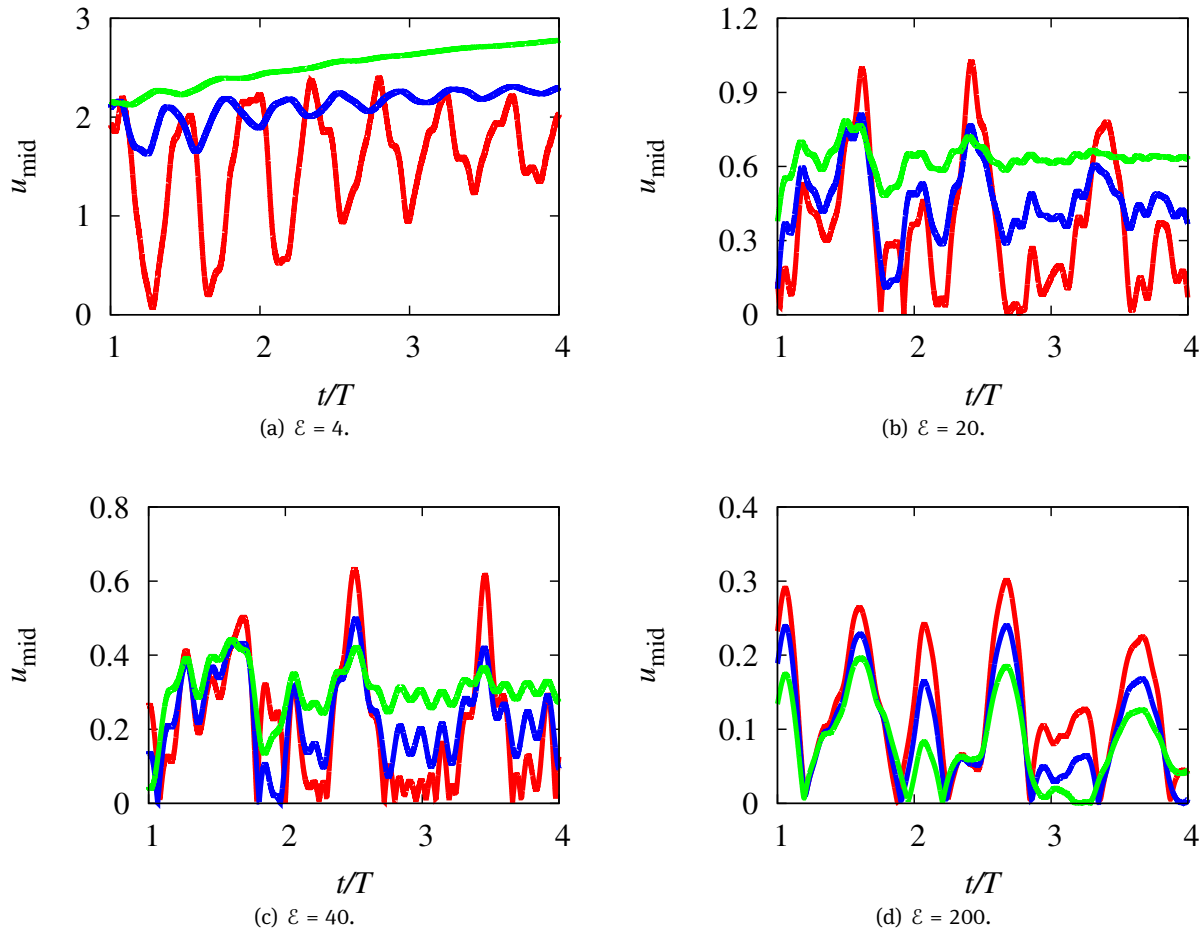


**Figure 3:** Time history of the displacement for different values of  $\varepsilon$  at  $\mathcal{R} = 15$  (green curve),  $\mathcal{R} = 50$  (blue curve) and  $\mathcal{R} = 100$  (red curve).

the TDG method. Such method is third order accurate and dissipative in the high frequency modes. The adopted TDG method and its superior properties with respect to Newmark or  $\alpha$  time integration schemes have been widely discussed and investigated in [52] within the fluid-structure interaction framework.

The initial configuration of the body is generated by using the software Gmsh [53]. Specifically, a spline line connects the three control points located at  $(\frac{L-l}{2}, 0)$ ,  $(\frac{l}{2}, h)$  and  $(\frac{L+l}{2}, 0)$ , respectively.

### 3 Results and discussion

Here, results from a numerical campaign are discussed. The peak value of the inlet velocity profile is set to  $V = 0.05$ . The corresponding Mach number is  $\mathcal{M} = \frac{V}{c_s} = 0.087$ , which represents a low value annihilating dele-

rious compressibility effects [38]. Moreover, the distance  $l$  is set to 50 lattice units. By varying the relaxation parameter  $\tau$ , scenarios characterized by different Reynolds numbers are achieved, i.e.  $\mathcal{R} = 15, 50, 100$ . Moreover, the role of the dimensionless elastic modulus, which assumes the values of  $\varepsilon = 4, 20, 40, 200$ , is dissected. All the simulations are characterized by  $m = 124.8$ ,  $A = 16$  and  $J = 21.33$ . All the results are presented in lattice units. To perform a conversion from the LB system to the real physical world, the author selects a scale factor for the length  $S_l = 1 \text{ m}/l = 0.02 \text{ m}$ , one for the velocity  $S_v = 1 \frac{\text{m}}{\text{s}}/V = 20 \frac{\text{m}}{\text{s}}$  and one for the density  $S_\rho = 1000 \frac{\text{kg}}{\text{m}^3}$  (with  $\rho = 1$ ). Consistently, all the other scaling factors can be easily derived, e.g.

- $S_t = S_l/S_v = 1 \times 10^{-3} \text{ s}$  for the time  $t$ ;
- $S_\nu = S_l S_v = 0.4 \text{ m}^2/\text{s}$  for the fluid kinematic viscosity  $\nu$ ;
- $S_a = S_l^2 = 4 \times 10^{-4} \text{ m}^2$  for the cross-sectional area  $A$ ;

- $S_j = S_l^4 = 1.6 \times 10^{-7} \text{ m}^4$  for the cross-sectional inertia  $J$ ;
- $S_e = S_\rho S_V^2 = 4 \times 10^5 \frac{\text{N}}{\text{m}^2}$  for the elastic modulus  $E$ ;
- $S_\psi = S_\rho S_l^{-3} S_V^2 = 5 \times 10^{10} \text{ J}$  for the energy  $\Psi$ .

These scale factors have been applied for all the simulations discussed in the present paper (even in Appendix). Firstly, the value of the aspect ratio is set to  $\mathcal{H} = 0.3$ . By defining the potential energy associated with the deformation of the beam as

$$\Psi = \frac{1}{2} \int_s \mathbf{U}^T \mathbf{K} \mathbf{U}, \quad (11)$$

in Figure 2 the time histories of this quantity are plotted. In the following,  $T$  denotes the first period of vibration of the solid body.

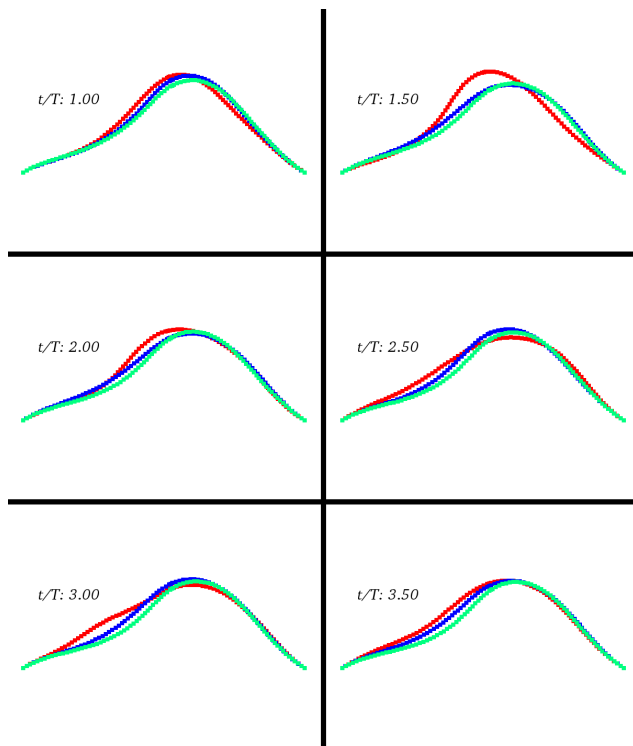


**Figure 4:**  $\varepsilon = 4$ . Configuration assumed by the solid body at different time instants at  $\mathcal{R} = 15$  (green curve),  $\mathcal{R} = 50$  (blue curve) and  $\mathcal{R} = 100$  (red curve).

For completeness, the velocity field is reported in Figure 6 for  $\varepsilon = 4$ .

As it is possible to observe, the solution of the problem drastically varies with the dimensionless quantities  $\mathcal{R}$  and  $\varepsilon$ . In particular, the higher  $\varepsilon$ , the lower the energy is. Concerning the scenario at  $\varepsilon = 200$ , a scaling-up of the energy with  $\mathcal{R}$  is experienced. In particular, the time histories of  $\Psi$  are characterized by the identical qualitatively poly-

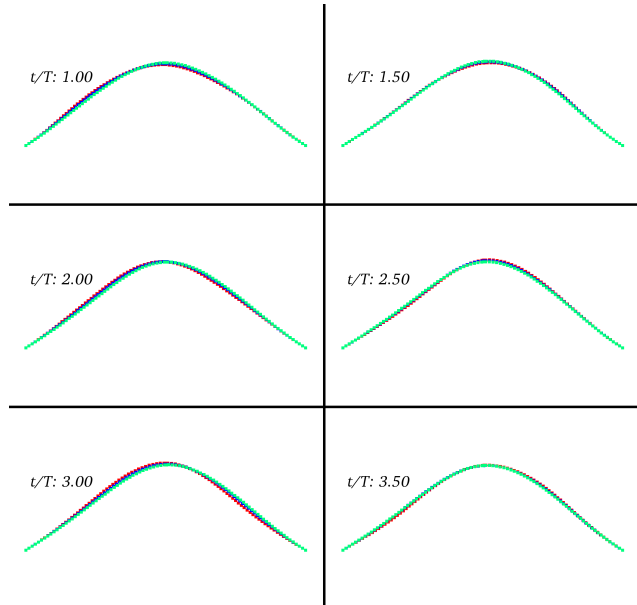


**Figure 5:**  $\varepsilon = 40$ . Configuration assumed by the solid body at different time instants at  $\mathcal{R} = 15$  (green curve),  $\mathcal{R} = 50$  (blue curve) and  $\mathcal{R} = 100$  (red curve).

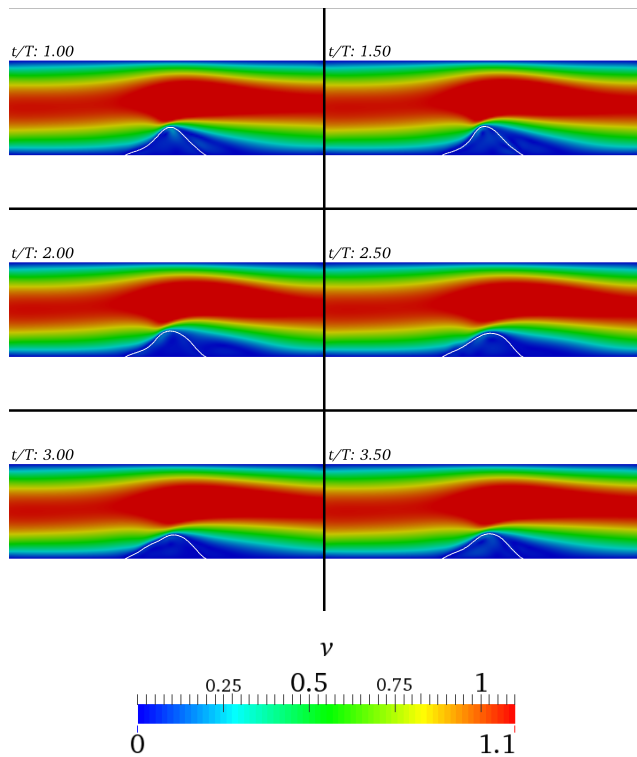


**Figure 6:**  $\varepsilon = 4$  and  $\mathcal{R} = 100$ . Velocity field at different time instants (normalized with respect to  $V$ ).

chromatic trend and only the amplitude varies, which increases with the Reynolds number. This tendency is found at  $\varepsilon = 200$ , where high-frequency oscillations manifest.

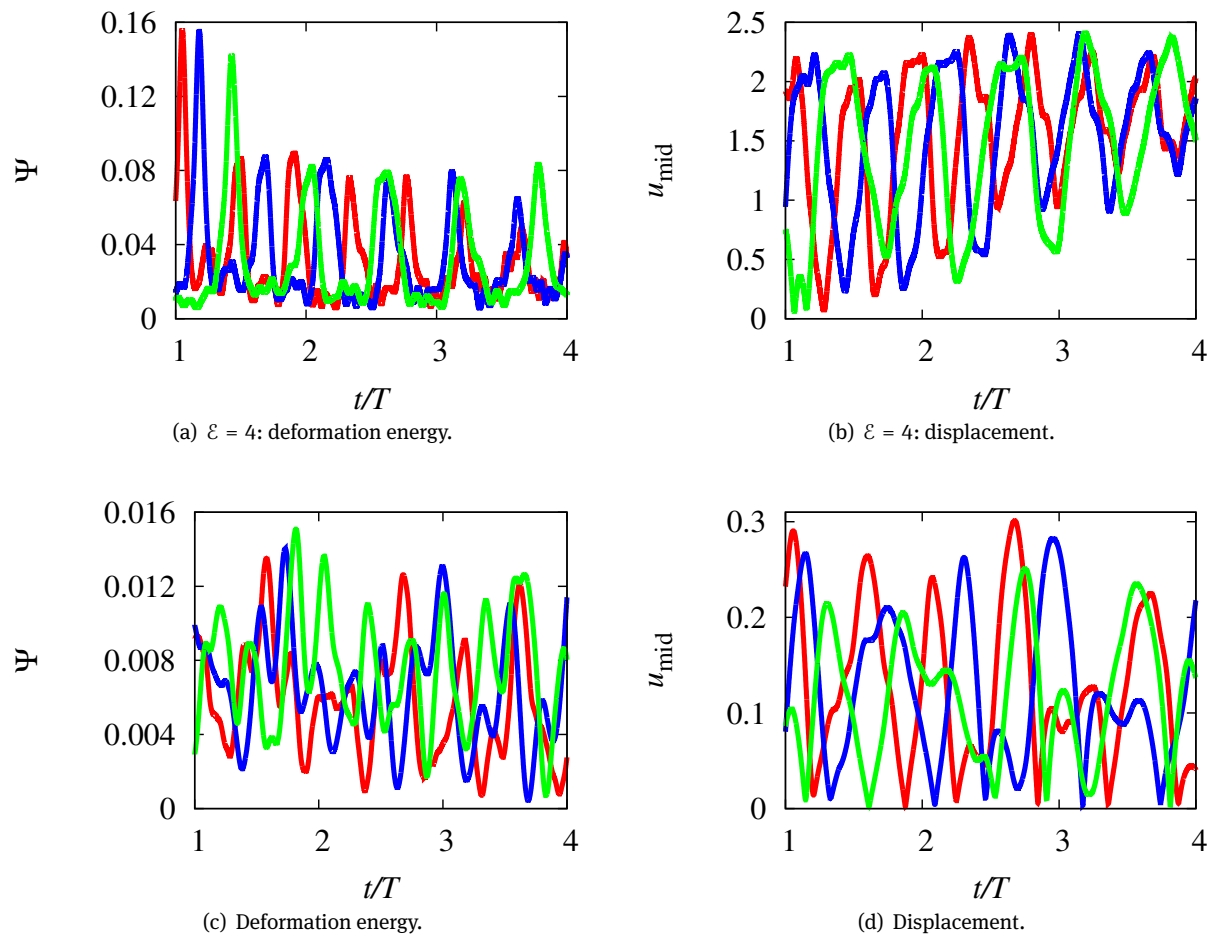


**Figure 7:** Time history of the deformation energies for different values of  $\mathcal{R}$  at  $\mathcal{D} = 7.8$  (red curve),  $\mathcal{D} = 10$  (blue curve) and  $\mathcal{D} = 15$  (green curve). All the simulations are characterized by  $\mathcal{R} = 100$  and  $\varepsilon = 200$ .

As  $\varepsilon$  reduces, the behaviour drastically varies. Specifically, for  $\varepsilon = 20$  progressively smoother time histories of  $\Psi$  are experienced as  $\mathcal{R}$  reduces. In particular, notice that the amplitude of the oscillations decreases in time and, especially for the lowest value of  $\mathcal{R}$ , the solution appears to plateau. This behaviour is emphasized at  $\varepsilon = 4$ , where the energy oscillations are definitely damped in time. A peculiar progression is found at  $\mathcal{R} = 15$ , where the energy highly differs from the other configurations. In fact, a quasi-static load is applied to the body, whose value is considerably higher with respect to the remaining scenarios. In the limit  $\mathcal{R} \rightarrow 0$ , the flow physics is highly smooth and stationary. Therefore, the system can be idealized as a structure undergoing a constant load and the dynamics solution approaches the static one. As  $\mathcal{R}$  assumes larger values, a more complex fluid dynamics manifests. The encompassing flow field is strictly unsteady and the resultant hydrodynamic loads evolve in time as well. These re-

sults are confirmed in Figure 3, where the time history of the mid-point displacement,  $u_{\text{mid}}$ , is reported for the above discussed configuration. In particular, it is interesting to notice that the multi-harmonic and stationary trends of the deformation energy clearly reflect the time history of the displacement.

In Figure 4, the configuration assumed by the solid body is reported at different time instants at  $\varepsilon = 4$ . It is worth to notice that the deformed configuration at  $\mathcal{R} = 100$  highly evolves in time, thus resulting in complex shapes assumed by the body. As  $\mathcal{R}$  reduces, the deformation appears progressively smoother. For comparison, the deformed configuration is reported in the scenario characterized by  $\varepsilon = 40$  at the same time instants in Figure 5. It appears immediately that a pretty steady dynamics affects the solid body.

The scenario characterized by  $\varepsilon = 200$  and  $\mathcal{R} = 100$  is selected to elucidate the role of the density and aspect



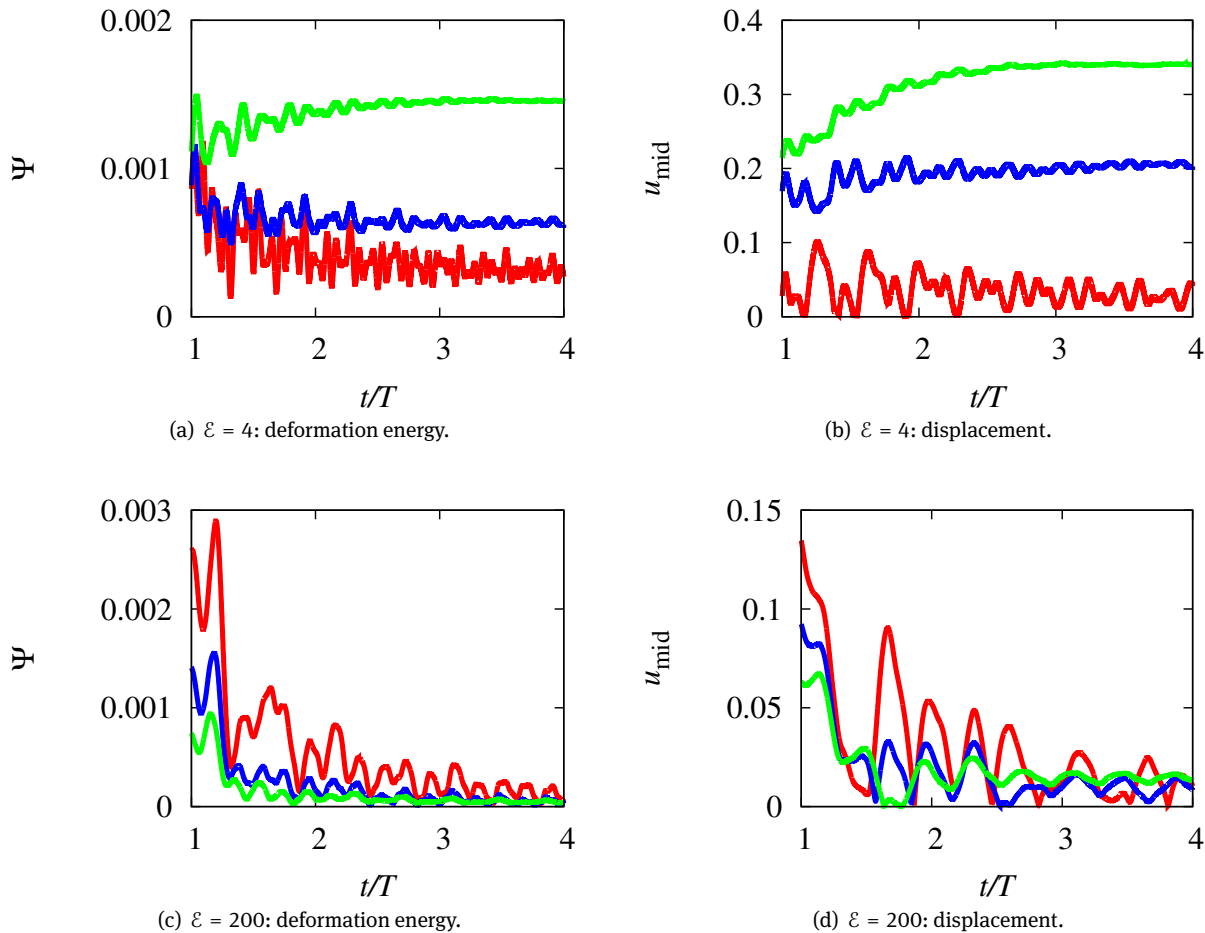


**Figure 8:** Time history of deformation energy and mid-point displacement at  $\mathcal{R} = 15$  (green curve),  $\mathcal{R} = 50$  (blue curve) and  $\mathcal{R} = 100$  (red curve). All the simulations are characterized by  $\mathcal{R} = 100$ .

ratios. In Figure 7, the time history of  $\Psi$  and the one of the mid-point displacement are reported for different values of  $\mathcal{D}$ , i.e.  $\mathcal{D} = 7.8, 10, 15$ . Substantially, the solutions are characterized by comparable amplitudes and frequencies. A similar trend is experienced for the remaining configurations. In the range of variations of the adopted dimensionless parameters, the author can conclude that the flow-induced vibrations are not significantly affected by the mass structural density.

On the other hand, the effect on the vibration regime of the  $\mathcal{H}$  appears highly prominent. In particular, the previously discussed solution at  $\mathcal{H} = 0.3$  are compared to the one obtained for a reduced value, i.e.  $\mathcal{H} = 0.15$ . The time history of  $\Psi$  and  $u_{\text{mid}}$  are reported in Figure 8 for different values of  $\mathcal{R}$ . Firstly, notice that the peak amplitudes of the two monitored quantities are remarkably lower than the corresponding ones at  $\mathcal{H} = 0.3$ . Moreover, it is intriguing to notice that the solution is highly damped and the curves

tend to plateau, especially as  $\mathcal{R}$  reduces. Finally, the above mentioned scaling-up with the Reynolds number is herein found too.

## 4 Conclusions

Here, the results of a numerical campaign investigating curved deformable body undergoing non-linear vibrations regimes induced by a flow have been reported. With respect to the existing literature and previous efforts, the present paper represents a remarkable upgrade. In fact, the author proposes that the problem is strongly (though not exclusively) dependent on the Reynolds number,  $\mathcal{R}$ . Moreover, the numerical campaign highlights that the role on the resultant solid dynamics of other three dimensionless parameters, i.e.  $\mathcal{H}$ ,  $\mathcal{D}$  and  $\varepsilon$ . These statements are assessed in the present paper for the first time. As demon-

strated, the vibration regime is drastically affected by the encompassing flow physics, which, in turn, depends on the position and velocity of the immersed solid body. From the purely *fluid* point of view, the body represents an obstacle that obstructs the flow, thus resulting in a severe modification of the fluid dynamics. In other words, as the initial solid configuration varies, the flow physics and the velocity field changes as well. Obviously, the non-linear vibration regime is consistently perturbed.

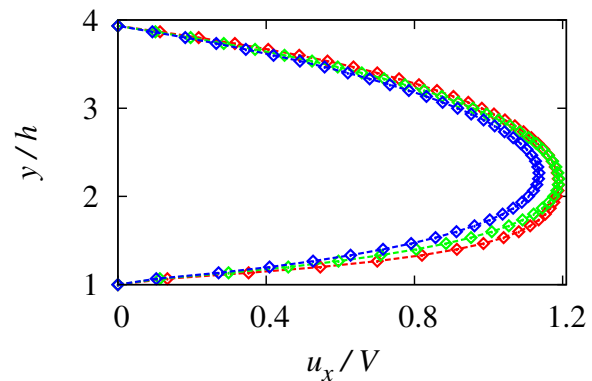
## Appendix: Validation

The proposed approach for immersed curved body is validated by comparing present results against the ones achieved by the commercial software Fluent [54]. Specifically, a rigid solid body with  $\mathcal{H} = 0.3$  invested by a flow is considered. In Figure 9, the components of the velocity vector at the vertical section located at  $x = L/2$  are depicted for different values of the Reynolds number. Diamonds and dashed lines identify the present and reference solutions, respectively. As it is possible to observe, a very strict close agreement is found.

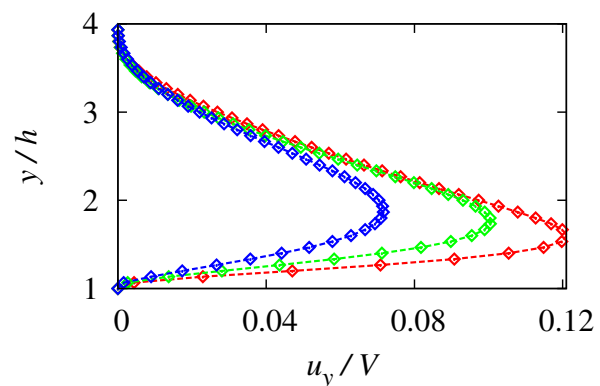
**Acknowledgement:** The authors would like to thank Prof. Serguei Iakovlev for the useful and motivating discussions. The author is also grateful to the editor and the reviewers for their comments, which improved the quality of the manuscript.

## References

- [1] Qin Z., Batra R.C. Local slamming impact of sandwich composite hulls. *Int. J. Solids Struct.*, 2009, 46, 2011-2035.
- [2] Panciroli R., Abrate S., Minak G., Zucchelli A. Hydroelasticity in water-entry problems: Comparison between experimental and SPH results. *Compos. Struct.*, 2012, 94, 532-539.
- [3] Panciroli R., Abrate S., Minak G. Dynamic response of flexible wedges entering the water. *Compos. Struct.*, 2013, 99, 163-171.
- [4] Shrivastava S., Mohite P.M. Redesigning of a canard control surface of an advanced fighter aircraft: Effect on buckling and aerodynamic behavior. *Curved and Layer. Struct.*, 2015, 2, 183-193.
- [5] Ke L., Yang J., Kitipornchai S. An analytical study on the nonlinear vibration of functionally graded beams. *Meccanica*, 2010, 45, 743-752.
- [6] Tornabene F., Fantuzzi N., Baccocchi M. Free vibrations of free-form doubly-curved shells made of functionally graded materials using higher-order equivalent single layer theories. *Compos. Part B*, 2014, 67, 490-509.
- [7] Amabili M. Nonlinear vibrations of laminated circular cylindrical shells: comparison of different shell theories. *Compos. Struct.*, 2011, 94, 207-220.
- [8] Viola E., Tornabene F., Fantuzzi N. General higher-order shear deformation theories for the free vibration analysis of completely doubly-curved laminated shells and panels. *Compos. Struct.*, 2013, 95, 639-666.
- [9] Natarajan S., Ferreira A.J.M., Nguyen-Xuan H. Analysis of cross-ply laminated plates using isogeometric analysis and unified formulation. *Curved and Layer. Struct.*, 2015, 1, 1-10.
- [10] Sahoo S. Free vibration behavior of laminated composite stiffened elliptic parabolic shell panel with cutout. *Curved and Layer. Struct.*, 2015, 2, 162-182.
- [11] Liu B., Xing Y.F., Qatu M.S., Ferreira A.J.M. Exact characteristic equations for free vibrations of thin orthotropic circular cylindrical shells. *Compos. Struct.*, 2012, 94, 484-493.
- [12] Pellicano F., Amabili M., Paidoussis M.P. Effect of the geometry on the non-linear vibration of circular cylindrical shells. *Int. J. Nonlin. Mech.*, 2002, 37, 1181-1198.
- [13] Gonçalves P.B., Del Prado Z.G. Effect of non-linear modal interaction on the dynamic instability of axially excited cylindrical shells. *Comput. Struct.*, 2004, 82, 2621-2634.



(a) Profile of the horizontal component of the velocity ( $u_x$ ).



(b) Profile of the vertical component of the velocity ( $u_y$ ).

**Figure 9:** Profiles of the components of the velocity vector at the vertical section located at  $x = L/2$  for different values of the Reynolds number, i.e.  $\mathcal{R} = 15$  (green), 50 (blue), 100 (red). Reference solutions and present findings are indicated by dashed lines and diamonds, respectively



- [14] Ferreira A.J.M., Carrera E., Cinefra M., Viola E., Tornabene F., Fantuzzi N., Zenkour A.M. Analysis of thick isotropic and cross-ply laminated plates by generalized differential quadrature method and a unified formulation. *Compos. Part B*, 2014, 58, 544-552.
- [15] Kubenko V.D., Kovalchuk P.S., Kruk L.A.. Nonlinear vibrations of cylindrical shells filled with a fluid and subjected to longitudinal and transverse periodic excitation. *Int. Appl. Mech.*, 2010, 46, 186-194.
- [16] Firouz-Abadi R.D., Noorian M.A., Haddadpour H. A fluid-structure interaction model for stability analysis of shells conveying fluid. *J. Fluid Struct.*, 2010, 26, 747-763.
- [17] Amabili M., Pellicano F., Paidoussis M.P. Non-linear dynamics and stability of circular cylindrical shells containing flowing fluid. Part I: stability. *J. Sound Vib.*, 1999, 225, 655-699.
- [18] Amabili M., Pellicano F., Paidoussis M.P. Non-linear dynamics and stability of circular cylindrical shells containing flowing fluid. Part II: large-amplitude vibrations without flow. *J. Sound Vib.*, 1999, 228, 1103-1124.
- [19] Amabili M., Pellicano F., Paidoussis M.P. Non-linear dynamics and stability of circular cylindrical shells containing flowing fluid. Part III: truncation effect without flow and experiments. *J. Sound Vib.*, 2000, 237, 617-640.
- [20] Amabili M., Pellicano F., Paidoussis M.P. Non-linear dynamics and stability of circular cylindrical shells containing flowing fluid. Part IV: large-amplitude vibrations with flow. *J. Sound Vib.*, 2000, 237, 641-666.
- [21] Karagiozis K.N., Amabili M., Paidoussis M.P., Misra K. Non-linear vibrations of fluid-filled clamped circular cylindrical shells. *J. Fluid Struct.*, 2005, 21, 579-595.
- [22] Karagiozis K.N., Amabili M., Paidoussis M.P., Misra K. Effect of geometry on the stability of cylindrical clamped shells subjected to internal fluid flow. *Comput. Struct.*, 2007, 85, 645-659.
- [23] Del Prado Z.J.G.N., Gonçalves P.B., Paidoussis M.P. Non-linear vibrations and imperfection sensitivity of a cylindrical shell containing axial fluid flow. *J. Sound Vib.*, 2009, 327, 211-230.
- [24] Amabili M., Karagiozis K.N., Paidoussis M.P. Effect of geometric imperfections on non-linear stability of circular cylindrical shells conveying fluid. *Int. J. Nonlin. Mech.*, 2009, 44, 276-289.
- [25] Iakovlev S., Seaton C.T., Sigrist J.F. Submerged circular cylindrical shell subjected to two consecutive shock waves: Resonance-like phenomena. *J. Fluid Struct.*, 2013, 42, 70-87.
- [26] Iakovlev S., Mitchell M., Lefieux A., Murray R.. Shock response of a two-fluid cylindrical shell system containing a rigid core. *Comput. Fluids*, 2014, 96, 215-225.
- [27] Bochkarev S.A., Lekomtsev S.V., Matveenkov V.P.. Natural vibrations of loaded noncircular cylindrical shells containing a quiescent fluid. *Thin Wall. Struct.*, 2015, 90, 12-22.
- [28] Fu Y, Price W.G.. Interactions between a partially or totally immersed vibrating cantilever plate and the surrounding fluid. *J. Sound Vib.*, 1987, 118, 495-513.
- [29] Kovalchuk P.S., Podchasov N.P. Stability of elastic cylindrical shells interacting with flowing fluid. *Int. Appl. Mech.*, 2010, 46, 60-68.
- [30] Breslavsky I.D., Strelnikova E.A., Avramov K.V. Dynamics of shallow shells with geometrical nonlinearity interacting with fluid. *Comput. Struct.*, 2011, 89, 496-506.
- [31] Kubenko V.D., Kovalchuk P.S., Podchasov N.P. Analysis of non-stationary processes in cylindrical shells interacting with a fluid flow. *Int. Appl. Mech.*, 2011, 46, 1119-1131.
- [32] Kovalchuk P.S., Podchasov N.P. Influence of initial deflections on the stability of composite cylindrical shells interacting with a fluid flow. *Int. Appl. Mech.*, 2011, 46, 902-911.
- [33] Kovalchuk P.S., Kruk L.A., Pelykh V.A. Stability of differently fixed composite cylindrical shells interacting with fluid flow. *Int. Appl. Mech.*, 2014, 50, 664-676.
- [34] Avramov K.V., Strelnikova E. A., Pierre C. Resonant many-mode periodic and chaotic self-sustained aeroelastic vibrations of cantilever plates with geometrical non-linearities in incompressible flow. *Nonlinear Dynam.*, 2012, 70, 1335-1354.
- [35] Avramov K.V., Strelnikova E. A. Chaotic oscillations of plates interacting on both sides with a fluid flow. *Int. Appl. Mech.*, 2014, 50, 303-309.
- [36] Higuera F.J., Succi S., Benzi R.. Lattice gas dynamics with enhanced collisions. *Europhys. Lett.*, 1989, 9, 345-349.
- [37] Benzi R., Succi S., Vergassola M. The lattice Boltzmann equation: theory and applications. *Phys. Rep.*, 1992, 222, 145-197.
- [38] Succi S. *The Lattice Boltzmann Equation for Fluid Dynamics and Beyond*. Clarendon, 2001.
- [39] Chen H., Chen S., Matthaeus W.H. Recovery of the Navier-Stokes equations using a lattice-gas Boltzmann method. *Phys. Rev. Lett.*, 1992, 5, R5339-R5342.
- [40] Fadlun E.A., Verzicco R., Orlandi P., Mohd-Yusof J. Combined immersed-boundary finite-difference methods for three-dimensional complex flow simulations. *J. Comput. Phys.*, 2000, 161, 35-60.
- [41] Peskin C.S. The immersed boundary method. *Acta Num.*, 2002, 11, 479-517.
- [42] Wu J. and Shu C. Implicit velocity correction-based immersed boundary-lattice Boltzmann method and its applications. *J. Comput. Phys.*, 2009, 228, 1963-1979.
- [43] Sotiropoulos F., Yang X.. Immersed boundary methods for simulating fluid-structure interaction. *Progr. Aerosp. Sci.*, 2014, 65, 1-21.
- [44] Filippova O., Hanel D. Lattice Boltzmann simulation of gas-particle flow in filters. *Comput. Fluids*, 1997, 26, 697-712.
- [45] De Rosi A. Harmonic oscillations of laminae in non-Newtonian fluids: A lattice Boltzmann-immersed boundary approach. *Adv. Wat. Resour.*, 2014, 73, 97-107.
- [46] Felippa C.A., Haugen B. A unified formulation of small-strain corotational finite elements: I. Theory. *Comput. Method. Appl. M.*, 2005, 194, 2285-2335.
- [47] Garcea G., Madeo A., Zagari G., Casciaro R. Asymptotic post-buckling fem analysis using corotational formulation. *Int. J. Solids Struct.*, 2009, 46, 377-397.
- [48] De Rosi A. A lattice Boltzmann model for multiphase flows interacting with deformable bodies. *Adv. Wat. Resour.*, 2014, 73, 55-64.
- [49] De Rosi A. On the dynamics of a tandem of asynchronous flapping wings: Lattice Boltzmann-immersed boundary simulations. *Physica A*, 2014, 410, 276-286.
- [50] De Rosi A. Fluid forces enhance the performance of an aspirant leader in self-organized living groups. *PloS ONE*, 2014, 9, e114687.
- [51] De Rosi A. Ground-induced lift enhancement in a tandem of symmetric flapping wings: Lattice Boltzmann-immersed boundary simulations. *Comput. Struct.*, 2015, 153, 230-238.
- [52] De Rosi A., Falcucci G., Ubertini S., Ubertini F. A coupled lattice Boltzmann-finite element approach for two-dimensional fluid-structure interaction. *Comput. Fluids*, 2013, 86, 558-568.

- [53] Geuzaine C., Remacle J.F. Gmsh: A 3-d finite element mesh generator with built-in pre-and post-processing facilities. *Int J. Numer. Meth. Eng.*, 2009, 79, 1309-1331.
- [54] FLUENT User Guide. Fluent inc. Lebanon NH, 2005, 3766.